Ultrahigh-resolution study of autodetachment in C_2^-

U. Hefter,* Roy D. Mead, P. A. Schulz,† and W. C. Lineberger
Department of Chemistry, University of Colorado, Boulder, Colorado 80309
and Joint Institute for Laboratory Astrophysics, University of Colorado
and National Bureau of Standards, Boulder, Colorado 80309
(Received 21 January 1983)

We describe a new coaxial laser—ion-beam photodetachment spectrometer designed to measure high-resolution photodetachment spectra of negative ions, and the measurement of C_2^- autodetachment rates with it. The apparatus resolution of 10 MHz is sufficient to resolve linewidth and line shape of autodetaching resonances in C_2^-. Autodetachment rates of the $B\ ^2\Sigma_u^+$ state have been measured for a variety of rotational levels with $v'=6$, 7, 8, and 9. The observed rates vary between 10^7 and $10^{10}\ s^{-1}$, depending on vibrational and rotational state. Autodetachment of high vibrational levels ($v'=19$) of the $A\ ^2\Pi_u$ state has been seen to be slower than $10^8\ s^{-1}$. The physical processes giving rise to these results are discussed in some detail.

I. INTRODUCTION

Experimental and theoretical investigations of interactions between electrons and atoms and between electrons and molecules have been one of the major topics in atomic physics. Electron scattering[1]

$$A+e^-\rightarrow(A^-)^*\rightarrow A+e^- \tag{1}$$

is the basic approach to study those interactions and has done much to increase our basic understanding. An alternative approach, the photodetachment of negative ions,

$$A^-+h\nu\rightarrow(A^-)^*\rightarrow A+e^- \tag{2}$$

often referred to as a half-collision process, allows electron-atom and electron-molecule interactions to be probed with the very high-energy resolution and selection rules characteristic of optical spectroscopy.

Resonance phenomena due to a short-lived collision complex, here an excited state of the negative ion interacting with the continuum of neutral plus electron, are very sensitive probes to investigate the nature of those interactions. Such resonances have been observed frequently in photoionization[2] and in electron scattering experiments.[1,2] Photodetachment resonances were first observed in alkali-metal negative ions[3] and have since been seen in many other atomic and molecular negative ions.[4,5]

Both the theoretical understanding of autoionization processes and the experimental capabilities necessary for their study have advanced tremendously over the past 20 years. The general problem of bound states embedded in continua was examined by Fano[6] in a classic 1961 paper. His treatment of a model system gave the general relationships between line profiles, intensities, resonance widths, and scattering phase shifts. Configuration interaction can mix bound and continuum states, allowing decay of multiply excited states if there is enough electronic energy to eject an electron. The mechanism by which vibrational energy is transferred into electronic degrees of freedom to produce autodetachment has been treated[7–9] as a special case of Born-Oppenheimer breakdown, in which nuclear kinetic-energy terms connect the bound and continuum states. The case of rotation-electronic coupling[8] has received less attention, since it has been assumed to play a comparatively minor role in autoionization if other mechanisms are active.

The autoionization of Rydberg states of H_2 has received particular attention, since H_2 is the simplest autoionizing molecular system. Experimental results of Herzberg[10] motivated Fano[11] to develop a form of multichannel quantum-defect theory for the H_2 autoionization problem, including the effects of rotational coupling between different autoionizing levels. Further theoretical work[12] has allowed proper interpretation of the data of Herzberg and Jungen[13] and Dehmer and Chupka.[14]

The motion of a Rydberg electron is only weakly coupled to the motion of the positive-ion core, although the long-range Coulomb field supports an infinite number of bound states. The weak coupling makes the ion core closely resemble the final ion state, giving rise to strong propensity rules[8] governing autoionization transitions. These propensity rules give preference to transitions where the vibrational and rotational levels of the core are unchanged.

Because there is no strong Coulomb field binding the electron to the core, the autodetachment of negative ions involves valence electrons and differs qualitatively from the autoionization of Rydberg levels. The autodetaching valence electron in a negative ion is strongly correlated with the ion core, although the long-range forces between the electron and the core do not support Rydberg-type bound states. The potential curve for the autodetaching negative-ion state generally bears little resemblance to the curve for the final neutral state. The propensity rules for vibration break down completely, and are replaced by a more general requirement for overlap of vibrational wave functions.[8,9] The rotational propensity rules are determined by a preference for low orbital angular momentum in the departing electron since this reduces the centrifugal

barrier.

For a detailed study of resonance phenomena, photodetachment of diatomic negative ions offers a variety of advantages. First, by adapting the coaxial beam technique to photodetachment experiments, one is able to achieve resolution of better than 1 part in 10^7, i.e., one can measure the linewidth of autodetachment resonances narrower than 50 MHz. Second, spectroscopy and electron affinities of neutral diatomics can be well known, providing the necessary information on the possible final states. Third, due to the absence of Coulomb interactions between electrons and neutron atoms or molecules, electron affinities typically are less than a few electron volts, thus allowing most of the photodetachment experiments to be undertaken with visible light. Fourth, the lack of Rydberg states for negative ions and the conservation of angular momentum and parity allow simpler theoretical descriptions than in photoionization and scattering experiments. Finally, a variety of decay mechanisms of the excited negative-ion state, e.g., configuration interaction, vibration to electronic coupling or rotation to electronic coupling, can be studied.

The best studied diatomic negative ion is C_2^-. To date, it is the only experimentally observed molecular negative ion known[15,16] to have a stable bound excited electronic state connected to the ground state by a dipole-allowed transition. The electronic structure of C_2^- is similar to that of other isoelectronic 13 electron systems CN, N_2^+, and CO^+. Herzberg and Lagerqvist[15] were the first to observe the $B\,^2\Sigma_u^+$-$X\,^2\Sigma_g^+$ transitions of $^{12}C_2^-$ and $^{13}C_2^-$ in a flash discharge of methane and provided spectroscopic constants up to $v'=4$ of the upper state and $v''=3$ of the lower state. Photodetachment experiments[16] and matrix-isolation studies[17] confirmed the assignments made by Herzberg and Lagerqvist.[15] Feldmann[18] measured the electron affinity of C_2 in a low-resolution photodetachment experiment and reported the value $EA(C_2)=3.54 \pm 0.05$ eV. In their photodetachment experiment, Lineberger and Patterson[16] observed, in addition to the Herzberg and Lagerqvist bands of C_2^-, a series of unidentified resonances in the region around 16 400 cm^{-1}. Jones *et al.*[5] investigated the C_2^- photodetachment cross section between 14 000 and 20 000 cm^{-1} in high resolution ($\Delta\nu=0.4$ cm^{-1}) and identified the observed resonances as the $B\,^2\Sigma_u^+(v'\geq 5) \leftarrow X\,^2\Sigma_g^+(v''\geq 6)$ transition between high vibrational states of C_2^-, followed by autodetachment to C_2+e^-.

In addition to improved molecular constants for C_2^-, the work of Jones *et al.*[5] bounded the electron affinity of C_2 by $3.374 \leq EA(C_2) \leq 3.408$ eV. The higher electron affinity of 3.54 eV reported earlier by Feldmann[18] was attributed to the $a\,^3\Pi_u$ excited state of C_2. Jones *et al.*[5] also deduced a much faster autodetachment rate into the final state ($C_2\,^3\Pi_u + e$) than into the ($C_2\,^1\Sigma_g^+ + e$) state, and attributed the inability to observe the direct photodetachment process to poor vibrational overlap between the possible initial and final states. The actual shape and width of the autodetachment resonances was masked by the instrumental linewidth, and they could only give an upper bound of 7.5×10^{10} s^{-1} for the autodetachment rates. Recent photodetachment experiments,[19] carried out with the coaxial beam apparatus described in this paper, resolved the spin-rotation splittings of both Σ states and the hyperfine structure of $^{13}C_2^-$. The $A\,^2\Pi_u$ state of C_2^- could be observed[19] indirectly via perturbations in the $B\,^2\Sigma_u^+$-$X\,^2\Sigma_g^+$ bands, arising from vibronic spin-orbit and rotation-electronic interactions between the $A\,^2\Pi_u$ and $B\,^2\Sigma_u^+$ states. Laser-induced fluorescence experiments to determine the raditive lifetime of the C_2^- $B\,^2\Sigma_u^+$ state have been carried out by Leutwyler *et al.*,[20] who report a lifetime for $v'=0$ and 1 of 75 ns, or equivalently a radiative transition rate of 1.4×10^7 s^{-1}.

A newly designed coaxial beam apparatus, based on ideas first realized in the photodissociation apparatus of Huber *et al.*,[21] is used here to measure autodetachment rates of C_2^- for various vibrational and rotational states of the C_2^- $B\,^2\Sigma_g^+$ state. The coaxial beam configuration has many advantages over the crossed-beam device used previously. The sensitivity of coaxial beam instruments is inherently greater, since the overlap volume of the laser and ion beams can be increased tremendously. The resolution of the coaxial device is also enhanced due to velocity compression. The width of the ion-beam velocity distribution is reduced by acceleration to high energies, reducing the Doppler width far below room-temperature values. While tuning may still be accomplished by varying the laser frequency, holding the laser frequency fixed while scanning the ion velocity is often a more practicable and convenient method. The design of the coaxial beam photodetachment spectrometer and its performance is described in Secs. II and III. The improved resolution enabled improved understanding of the processes occurring in the ion source, resulting in reduced ion-energy spread and further improvement in resolution. The effects are discussed in Sec. IV. Finally Sec. V presents the experimental results of the C_2^- autodetachment rates and discusses their implications concerning the autodetachment process.

II. EXPERIMENTAL

The development of coaxial beam systems has been rapid, with progress occurring in several laboratories. Wing *et al.*[22] studied excitation of positive ions using laser and ion beams crossing at a small angle. Dufay *et al.*[23] have done saturation spectroscopy of atoms in a merged-beam system. Carrington and Sarre[24] have done absorption and photodissociation spectroscopy of ions using a double mass-spectrometer system with a coaxial laser-ion interaction region. Our instrument is similar to the apparatus at SRI used by Huber *et al.*[21] The SRI machine, used for ion spectroscopy and photodissociation studies, can determine the kinetic energies of charged dissociation products. It has also been used to study predissociation lifetimes and linewidths.[25]

Figure 1 shows the arrangement of the coaxial photodetachment apparatus used in this work. Basically, a mass-analyzed negative-ion beam is merged over the length of the interaction region with the beam of a tunable single-mode dye laser. The neutrals produced by photodetachment are detected to provide a direct measure of the relative photodetachment cross section. Instead of varying the frequency of the laser light to measure the energy

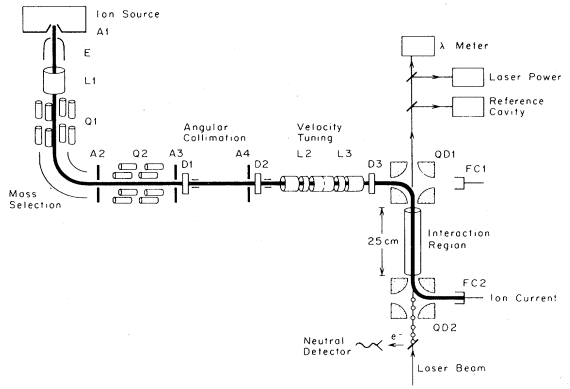

FIG. 1. Schematic of the coaxial beam photodetachment spectrometer. Einzel lenses and quadrupole lenses are designated by L and Q, respectively, apertures by A, the quadrupole deflectors by QD, the ion extractor by E, and the Faraday cups by FC.

dependence of the photodetachment cross section, the energy of the ions and thus the Doppler shift of the laser frequency is changed.

Generation of the mass-analyzed ion beam has been described in detail in earlier papers[5,26] and is reviewed here only briefly. A hot discharge ion source (shown in Fig. 2) operating with an equal mixture of acetylene and carbon monoxide at a total pressure of about 0.1 Torr is used to produce a C_2^- ion beam of ~ 0.3 nA. The negative ions are extracted from the hot discharge into the first stage of differential pumping (pressure 2×10^{-5} Torr) and are accelerated to their final energy E_0. All of the data reported in this paper were obtained with C_2^- beam of $E_0=3.8$-keV energy. An electrostatic quadrupole doublet lens ($Q1$) focuses the ion beam into a mass-analyzing 90° sector magnet. After passing through a differential pumping slit ($A2$), the mass-analyzed beam is recollimated by a second electrostatic quadrupole doublet lens ($Q2$) in a region ion pumped to 10^{-6} Torr. Two apertures ($A3$ and $A4$), 2 mm in diameter separated by 40 cm, limit the divergence of the ion beam to less than 0.6 deg. Horizontal and vertical deflectors ($D1$ and $D2$) help to direct the ion beam into the detachment chamber containing the coaxial laser—ion-beam spectrometer. The angular collimation region of the apparatus is differentially pumped by an ion pump reaching a pressure of 1×10^{-8} Torr.

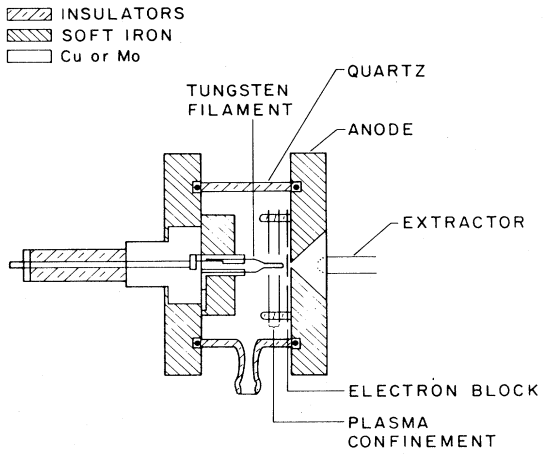

FIG. 2. The hot-cathode discharge ion source used in this work. The filament was held about 100 V negative with respect to the anode. The plasma confinement plates are electrically floating, while the electron block is connected to the anode. An axial field of about 300 G is applied by horseshoe magnets attached to the source.

Zeman[27] and Huber *et al.*[21] have demonstrated the electrostatic quadrupoles oriented perpendicularly to the bending plane are ideal devices to merge ion beams with neutral beams and to merge ion beams of opposite charge, and are obviously well suited for merging an ion beam with a laser beam. The major advantages of using quadrupole deflectors over other types of electrostatic or magnetic deflectors are that they are quite achromatic, they do not change the divergence of the ion beam, and they already have all the openings required to merge two beams.

The central components of our coaxial beam spectrometer consist of a zoom-einzel lens combination ($L2$ and $L3$) that enables us to change the energy of the ions, and the two quadrupole deflectors ($QD1$ and $QD2$) spaced by a 25-cm-long shielded interaction region. The zoom and einzel lens are operated as a five-element tube lens, sharing the center element. The zoom lens ($L2$) is basically a three-element asymmetric voltage lens that preserves the image at a fixed position, while allowing us to change the energy of the image by the potential difference between the first and third elements. The net effect is to produce a focus of the ion beam with energy E_0+eU, changing the energy of the ions by the float potential U. As a consequence of the energy change eU of the ions in the zoom lens, all following ion optical devices must be floated by the voltage U. The ion beam is recollimated by the einzel lens ($L3$) to its original divergence before it enters the first quadrupole deflector ($QD1$) that bends the ion beam through 90° and merges it with the laser beam. The ion and laser beam stay merged throughout the interaction region until they are separated by the second quadrupole deflector ($QD2$). A Faraday cup ($FC2$) located behind the deflector allows us to monitor the ion-beam current during the experiment. The quadrupole deflectors are of similar dimensions to those described in Ref. 27 but differ slightly in design in order to simplify construction. The main and shim electrodes as well as the mountings are made out of 6061 aluminum alloy. The alignment and electrical isolation of the electrodes is provided by spacers machined from polyimide (Dupont Vespel). To keep background count rates due to collisional detachment low the coaxial beam spectrometer is operated at a pressure of 3×10^{-10} Torr which is reached by an ion pump and an additional titanium sublimation pump.

The neutral particles produced in the interaction region by photodetachment do not recoil out of the ion beam as a result of the negligible transfer of momentum in the detachment process, but rather travel with the ions, pass the second deflector unaffected by its electrostatic field, and impact further downstream on a glass plate. (A tran-

sparent medium is necessary because neutrals and laser photons are still merged.) The neutrals impact the glass plate producing secondary electrons which are accelerated toward a Ceratron continuous-dynode particle multiplier operating in a single-particle counting mode. Use of a quartz plate gave rise to charging problems due to the high resistivity of quartz. This problem was remedied by replacing the quartz with an ordinary soda-lime glass microscope slide. The glass plate and Ceratron multiplier are mounted inside an aluminum box whose potential can be adjusted to avoid background counts. The efficiency of the neutral detector reaches $\sim 5\%$, as determined by comparing the measured O^- collisional stripping count rate with that estimated from known values of the absolute O^- collisional detachment cross section. A second detector to collect the detached electrons from the entire interaction volume has been developed, but was not yet ready to be used in the present experiment.[28]

The laser system used in this experiment consists of a single-mode dye laser (Spectra Physics Model 580) pumped by an argon-ion laser. The dye-laser frequency is actively stabilized by locking the dye-laser output to the side of a Fabry-Perot fringe of a stable reference cavity. This reduces the dye-laser frequency jitter to less than 10 MHz. The absolute frequency of the dye laser is measured with a λ meter[29] to an accuracy of 1 part in 10^6 (± 0.02 cm^{-1}). In contrast to earlier crossed-beam experiments,[5] the coaxial beam experiment is not performed inside a linear laser cavity because the counterpropagating waves inside the cavity appear as two different wavelengths to the moving ions, leading to a doubling of structure in the cross section. Moreover, the cavity mode spacing of the extended linear laser cavity would be too small to readily allow single-mode operation. A portion of the dye-laser output is used to supply laser stabilization and the λ meter, leaving roughly 20 mW of extracavity laser power for the photodetachment experiment.

The energy dependence of the photodetachment cross section can be measured either by changing the frequency of the laser light or by changing the velocity of the ions, thus changing the Doppler shift between molecular absorption and laser frequency. The coaxial beam spectrometer descirbed here was designed to scan the velocity (energy) of the ions. To accomplish this, the zoom lens (L 2) is set to decelerate the ions by reducing their energy by the float potential U. The outer sections of the quadrupole deflectors and the tube shielding the interaction region are floated to the voltage U and the einzel lens and quadrupole deflectors are adjusted to the new energy of the ions. Over the range of interest, the einzel and zoom lens voltages vary linearly with the float voltage. Thus a simple voltage divider chain, driven by the float voltage, can be used to ramp the ion optics. Typically, a 1-keV deceleration of the ions could be achieved without significant changes of the ion-beam properties. Tests made using a 2-keV O^- beam showed that the photodetachment signal as well as the background due to collisional detachment stayed constant within 5% over the range of the typical narrow Doppler scan. For the 3.8-keV C_2^- beam a deceleration scan of 1 keV corresponds to a frequency tuning through 1.4 cm^{-1}, slightly more than the 1-cm^{-1} tuning range of commercial dye lasers. The C_2^- photodetachment cross sections shown in this paper were obtained by scanning the energy of the ions through ~ 40 V.

The coaxial laser—ion-beam spectrometer is controlled by a PDP 8/E computer that scans the energy of the ions and collects all data from signal, background, and monitoring channels. Relative photodetachment cross sections are derived from the measured signal counts by subtracting collisional detachment and background counts and by normalizing to ion-beam current and photon flux. Count rates are ~ 50 kHz on strong C_2^- autodetachment resonances, 1 kHz of which are due to collisional detachment and a few Hz dark counts for a 0.3-nA ion beam and 20 mW of laser power. Typical integration times for the C_2^- spectra shown here are 1 s/channel.

III. RESOLUTION AND SENSITIVITY

The basic limitations to the resolution of tunable laser photodetachment experiments are Doppler broadening of the laser in the frame of the moving ion and the linewidth of the laser itself. Tunable single-mode dye lasers, covering the entire visible spectrum, are available today with a linewidth of the order of 1 MHz or less. As we will see, the laser linewidth is not the major factor limiting the resolution in this experiment. Of far more concern is, in this context, broadening due to the Doppler effect. In crossed-beam experiments this broadening results primarily from the angular divergence of the ion beam and is given by

$$\delta\nu = \frac{v}{\lambda}\sin\Delta\theta \approx \frac{v}{\lambda}\Delta\theta \ , \tag{3}$$

where $\delta\nu$ is the frequency width, v is the ion-beam velocity, λ is the laser wavelength, and $\Delta\theta$ is the full angle of beam divergence. Jones *et al.*[5] reported a Doppler width of 5.5 GHz for a 420-eV C_2^- beam in their crossed-beam instrument. Much higher resolution can be achieved by taking advantage of the features of the coaxial beam geometries, as was recognized quite early by Trujillo *et al.*[30] In such an arrangement the divergence $\Delta\theta$ of the ion beam contributes only as

$$\delta\nu = \frac{v}{\lambda}\left[1-\cos\frac{\Delta\theta}{2}\right] \approx \frac{v}{\lambda}\frac{(\Delta\theta)^2}{8} \tag{4}$$

to the resolution. A second factor, the velocity spread Δv of the ion beam, negligible in crossed-beam experiments, is directly related to the Doppler broadening in the coaxial apparatus

$$\delta\nu = \frac{\Delta v}{\lambda} \ , \tag{5}$$

and more serious to deal with. If we assume the C_2^- beam is the same as used by Jones *et al.*,[5] we expect Doppler broadening due to divergence and velocity spread of the ion beam of 60 and 230 MHz, respectively. This comparison does not show all the potential of the coaxial beam geometry, even though the resolution has been improved by a factor of 50. We can take further advantage of the velocity compression $\Delta v = \Delta E/\sqrt{2mE}$ by using ion beams of higher energy, together with a reduction of the

TABLE I. Contributions to the apparatus resolution for the crossed-beam experiment of Jones *et al.* (Ref. 5), hypothetical coaxial beam experiment using the ion-beam data from Ref. 5, and the coaxial beam experiment of the present work. The full width at half maximum (FWHM) energy spread ΔE and full angular divergence $\Delta\theta$ are estimates.[a] All linewidths are in MHz.

Type of Experiment	Crossed beams (Ref. 5)	Coaxial beams	Coaxial beams (This work)	
Ion-beam data				
E (eV)	420	420	3800	3800
ΔE (eV)	2.0	2.0	1.0	0.2
$\Delta\theta$ (deg)	4.7	4.7	0.6	0.6
Interaction length (mm)	1.0	300	300	300
Broadening due to				
Divergence of the ion beam	5500	60	0.6	0.6
Velocity spread of the ion beam	12	230	38	7.4
Interaction time	20	<0.1	0.2	0.2
Laser linewidth	10 000	10	<10	<10
Overall resolution (MHz)	12 000	240	40	12

[a]The data given in the last column describe the final resolution attained.

divergence $\Delta\theta$, and thus improve further the resolution. Table I lists the ion-beam parameters and the resulting broadening effects for the coaxial beam apparatus, and for comparison the corresponding data for the crossed-beam experiment of Jones *et al.*[5] The energy spread and divergence of the ion beam are conservative estimates. Increasing the beam energy by a factor of 9, to 3.8 keV, yields a reduction in the broadening due to velocity spread of a factor of 3. Collimation of the ion beam to $\Delta\theta=0.6$ deg makes divergence broadening negligible. As Table I further shows, transit-time broadening is of no concern for both types of experiments. Taking all broadening effects into account, we predict an overall resolution of 40 MHz for the coaxial beam apparatus. In fact the narrowest C_2^- autodetaching resonance we observed had a width of 12 MHz. Although the natural width of this resonance is not known, this observation confirms a resolution of the coaxial beam spectrometer of the order of 10 MHz, an improvement in resolution of three orders of magnitude over the earlier experiments.[5] This result also indicates that the actual energy spread of the ions has been improved to 0.2 eV from the originally obtained 2.0 eV. Further improvement, even to $\delta\nu=1$ MHz, seems feasible with the development of more monochromatic negative-ion sources.

In most experiments, an increase in resolution is directly related to a corresponding loss in sensitivity. This is not the case in the coaxial beams experiment, where the primary cause of loss of signal is the much lower laser power (20 mW compared to 20 W used in the crossed-beam experiment). Almost all of this signal loss is subsequently recovered due to the longer interaction time in the coaxial beam experiment. If we assume complete overlap of the 2-mm^2 ion and laser beam over the 300-mm interaction length, and (b) a 3-mm^3 interaction volume for the crossed-beam experiment, and take into consideration the higher ion-beam velocity in this experiment, we see that the loss in detachment rate would be roughly a factor of 10. In the crossed-beam C_2^- experiment[5] the laser linewidth was 12 GHz. The linewidth of the single-mode dye laser used in this experiment is narrower than the C_2^- resonances, so we gain a large factor from higher spectral power density. The sensitivity of the neutral particle detection system is about a factor of 20 times lower than the electron detection system previously used.[5] Considering all these factors, the present coaxial beam experiment is about as sensitive as the crossed-beam experiment.[5] Much higher sensitivities can be readily achieved by using ring dye lasers of typical 600-mW output power, utilizing an intracavity ring laser, and by using an efficient electron detector.[28]

IV. ENERGY SPREAD OF THE ION BEAM

The energy spread, i.e., the velocity distribution, of a negative-ion beam extracted from a hot discharge has not been quantitatively measured. Basically, it is of no great importance in crossed-beam experiments, but as pointed out in Sec. III, it is the resolution limiting factor in coaxial beam experiments. A 1-eV estimate for the source energy spread after acceleration to 3.8 keV ($v=1\times10^5$ m s^{-1}) leads to a velocity spread of 24 m s^{-1}, a 40-MHz linewidth. To measure the "real" shape of a resonance, it is also important to know the shape of the velocity distribution of the ion beam since the observed line shape is a convolution of the two.

The usual way to adjust the ion source is to tune for maximum beam current, generally resulting in operating the ion source at high pressures. Figure 3 shows a *single* C_2^- autodetachment resonance, taken at a source pressure of about 0.5 Torr, which splits into two peaks due to a double-peaked velocity distribution. Changing the propagation direction of the laser with respect to the ion-beam

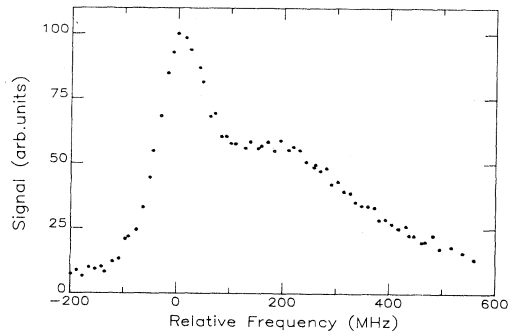

FIG. 3. Autodetachment resonance of C_2^- measured at high ion source pressure. The double-peak structure of the resonance is due to a double-peaked velocity distribution. Point spacing is 11 MHz.

velocity reverses the relative positions of the narrow and broad peaks, thus proving that this splitting is due to the velocity distribution. The narrower peak is due to the primary velocity distribution whereas the broad peak results from molecules with a velocity that is $\sim 90\ \mathrm{m\,s^{-1}}$ slower than the primary velocity of the ion beam. When the source pressure is lowered by a factor of 5 or more the broad peak disappears and a narrow, symmetric line around the primary velocity is all that remains. The intensity of the broad peak varies not only with source pressure but has been observed to be more prominent for high rotational states than for low ones. The buildup of a second velocity component in the ion-beam velocity distribution at high source pressures is due to an increasing number of inelastic collisions of the C_2^- ions with the source gas in the region between anode and extractor.

It has also been found that the large electric fields between the source filament and anode broaden the ion velocity distribution. The problem was remedied by making the "electron block" plate (shown in Fig. 2) cover a larger region around the ion extraction hole in the anode. This allows the ions to thermalize in a relatively field-free region before leaving the source.

V. DATA AND DISCUSSION

The photodetachment cross section of C_2^- in the range between 14000 and 20000 $\mathrm{cm^{-1}}$ has been measured at 0.4-$\mathrm{cm^{-1}}$ resolution by Jones *et al.*[5] and reported to be highly structured. The resonances creating this structure are explained by autodetachment of the C_2^- $B\,^2\Sigma_u^+$ state. Figure 4 (reproduced from Ref. 5) shows the C_2^- and C_2 potentials involved in the autodetachment process. Levels of the C_2^- $B\,^2\Sigma_u^+$ state with $v' \geq 5$ lie energetically above the onset of the C_2+e continuum and can autodetach to the C_2 $X\,^1\Sigma_g^+$ ground state, while for $v' > 5$ the C_2 $a\,^3\Pi_u$ state is also accessible. The C_2^- $B\,^2\Sigma_u^+$ autodetaching states are populated by the laser via bound-bound transitions from high vibrational levels of the C_2^- $X\,^2\Sigma_g^+$ ground state. In the earlier experiments[5] the rotational structure of the C_2^- $B\,^2\Sigma_u^+$-$X\,^2\Sigma_g^+$ transitions could be resolved, but due to the apparatus linewidth of 6 GHz, neither the spin-rotation splitting nor the natural

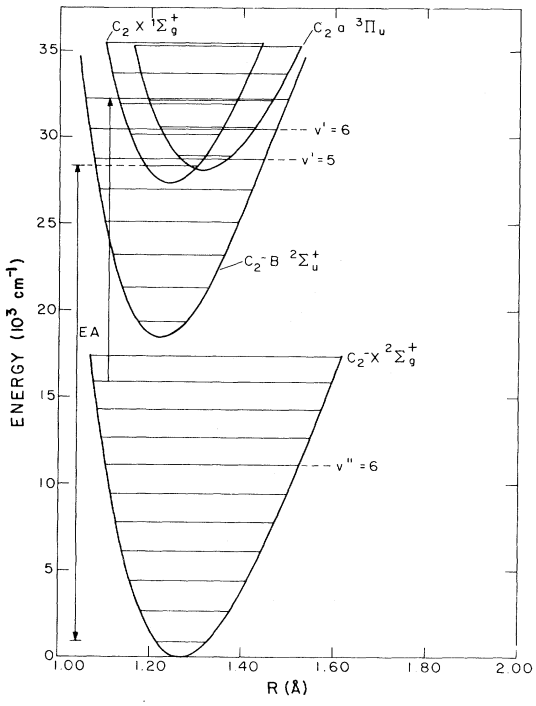

FIG. 4. RKR potential curves for X and B states of C_2^- and for X and a states of C_2; reproduced from Ref. 5. Vertical arrow indicates transitions of the C_2^- 7—9 band that were, among others, observed in this work.

linewidth of the resonances could be observed. With the coaxial beam apparatus, we have remeasured the C_2^- photodetachment cross section in the range of the $\Delta v = -2$ sequence band between 16000 and 17000 $\mathrm{cm^{-1}}$, and resolved the shapes and widths of individual autodetachment resonances. The presentation of the data has been divided into four parts. First (Sec. V A), we discuss the line shape of the observed C_2^- resonances. Section V B presents the vibrational and the rotational dependences of the autodetachment rates. Possible autodetachment mechanisms, explaining the observed behavior of the rates are discussed in Sec. V C. Finally, perturbations between the $B\,^2\Sigma_u^+$ and the $A\,^2\Pi_u$ state give some of the autodetaching $B\,^2\Sigma_u^+$ levels a substantial amount of Π character, enabling us to observe autodetachment of $A\,^2\Pi_u$ levels (Sec. V D).

A. Autodetachment line shape

The absorption profile of autoionizing or autodetaching lines, assuming energy-independent mixing of a single discrete state with one continuum having a constant density of states, is known to have a Fano line shape[6] in the energy region near the resonance

$$\sigma(\epsilon) = \sigma_b + \sigma_a(\epsilon+q)^2/(\epsilon^2+1)\ , \tag{6}$$

where $\epsilon = (E - E_0)/(h\Gamma/2)$ is the reduced energy variable, containing the energy E_0 and the width Γ of the resonance. The term q describes the asymmetry of the resonance, and its square is proportional to the ratio of the

transition probabilities between the initial state and the "modified" discrete state and to the continuum of bandwidth Γ; in other words, q^2 gives an estimate of the ratio of autodetachment to direct photodetachment. In the absence of an interference between direct transition and transition via the discrete state into the continuum, the Fano line shape reduces to a symmetric Lorentz profile ($q \rightarrow \infty$).

In C_2^-, direct photodetachment (which involves many more continua than the resonant one) is found[5] to be much weaker (by a factor of 10^3 or more) than autodetachment. We thus expect the autodetachment resonances to be nearly symmetric, and it should be possible to fit them with a Lorentzian profile, rather than a Fano interference profile. Figure 5 shows an ultrahigh-resolution scan of the C_2^- photodetachment cross section in the region of the $P_1(10)$ transition of the $v'=7$, $v''=9$ band. Because $^{12}C_2^-$ has no hyperfine structure ($I=0$), and spin-rotation splitting has been resolved, the width of this resonance reflects the autodetachment rate of the $v'=7$, $J'=9.5$, $N'=9$ level of the C_2^- $B\,^2\Sigma_g^+$ state. The experimental data are represented by the filled circles whereas the solid curve reflects a Fano profile giving the best fit to the data. The deviation in the fit is less than 1% of the peak height, just reflecting the signal-to-noise ratio (roughly 100/1) of the experiment. Within the limits set by the experimental signal-to-noise ratio, shown in Fig. 5, all observed autodetachment resonances show a symmetric Lorentz profile. This is reflected by a fitted asymmetry parameter q for the $P_1(10)$ resonance of greater than 100, a 10^4 times higher probability to detach the electron by autodetachment than by direct photodetachment. Since the profiles are all Lorentzian and the radiative lifetime of C_2^- is much longer[20] than the autodetachment lifetime, the width of resonances gives a direct determination of the decay rate. Although the width of the resonance (149 MHz) can be determined from the fit to ± 1 MHz, typical errors are ± 15 MHz due to uncertainties in the resolution of the apparatus and weak saturation of the detector. The resolution, i.e., the energy spread of the ions, may change due to varying conditions—such as contamination or different tunings—in the ion source.

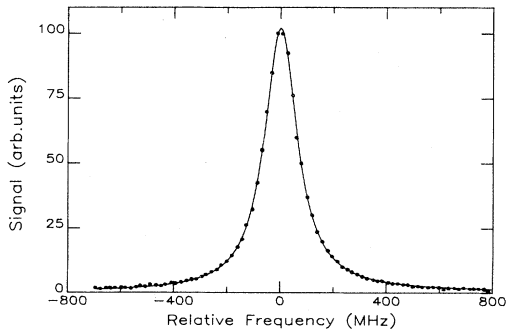

FIG. 5. Resonance of the C_2^- $B\,^2\Sigma_u^+ \leftarrow X\,^2\Sigma_g^+ : P_1(10)$ 7–9 transition at 16317.44 cm^{-1} due to autodetachment of the $B\,^2\Sigma_u^+$ $v'=7$, $J'=9.5$, $N'=9$ level. Solid line represents a virtually symmetric Fano profile with FWHM of 149 MHz, corresponding to an autodetachment rate of 9.4×10^8 s^{-1}. Point spacing is 19 MHz.

B. Vibrational and rotational dependence of the autodetachment rates

Autodetachment rates, i.e., the width of the autodetachment resonances, have been measured for 33 representative states covering vibrational levels $v'=5$–9 and molecular rotations from $N'=1$ to 51. Table II lists the autodetachment rates and the lifetimes of the autodetaching levels for different vibrational states. The rates have been calculated from the widths of transitions terminating in the $N'=19$ and $J'=19.5$ states. The lowest vibrational level of the C_2^- $B\,^2\Sigma_u^+$ manifold that can autodetach is $v'=5$. From an analysis of the observed intensity difference between resonances originating from the decay of the $v'=5$ level and those originating from the $v'=6$ level, Jones *et al.*[5] deduced that the autodetachment rate of $v'=5$ lies within the bounds (in units of s^{-1})

$$1\times10^6 \le \gamma_5 \le 1\times10^7 .$$

We have seen that the $v'=5$ autodetachment resonances are narrower than the resolution of our coaxial beams apparatus, corresponding to an autodetachment rate of less than 1×10^8 s^{-1}, consistent with the earlier result.[5] Autodetachment of the $v'=6$, $J'=19.5$ level has been measured to occur at a rate of 3.8×10^8 s^{-1}. The dramatic change (at least 40-fold) of the autodetachment rate between $v'=5$ and 6 is due to opening of a new detachment channel. Whereas $v'=5$ can detach only to the continua C_2 $X\,^1\Sigma_g^+ + e$, the additional final state C_2 $a\,^3\Pi_u + e$ becomes energetically accessible for autodetachment of $v' \ge 6$ levels. In the picture of single-electron molecular orbitals, autodetachment of the C_2^- $B\,^2\Sigma_u^+$ state to either C_2 $X\,^1\Sigma_g^+$ or C_2 $a\,^3\Pi_u$ requires a two-electron process. The *ab initio* calculations of Zeitz *et al.*[31] showed that strongly R-dependent configuration mixing in the C_2^- $B\,^2\Sigma_u^+$ state favored configurations of the form $\Pi_u \times \pi_g$, which may explain the much larger autodetachment rates to the C_2 $a\,^3\Pi_u$ over that to the C_2 $X\,^1\Sigma_g^+$ state.

The rates of autodetachment for the vibrational levels $v'=7$, 8, and 9 are by factors of 3.4, 8.4, and 23, respec-

TABLE II. C_2^- autodetachment rates and lifetimes experimentally determined for different vibrational levels. The rate of $v'=5$ is an upper bound from the work of Jones *et al.* (Ref. 5), whereas the rate of $v'=10$ is a lower bound due to the separation of unresolved rotational lines. All other data were taken for the rotational level $J=19.5$ and $N=19$. Typical errors are $\pm1\times10^8$ s^{-1}.

v'	Rate (s^{-1})	τ (ns)
5	$\le 1\times10^7$	≥ 100
6	3.8×10^8	2.6
7	1.3×10^9	0.8
8	3.2×10^9	0.31
9	8.7×10^9	0.1
10	$\ge 3.0\times10^{10}$	≤ 0.03

tively, faster than the rate for detachment of $v'=6$. Resonances due to autodetachment of $v'=10$ could also be observed in the photodetachment cross section but they overlap so badly that their spectroscopic assignment could not be accomplished. From known spectroscopic data for the lower vibrational levels, the line separation in the region of the unresolved bandhead of the $v''=12$, $v'=10$ transition is estimated to be at least 0.1 cm^{-1}. Since the spectrum is observed to be overlapping, this gives a lower bound of 3×10^{10} s^{-1} for the $v'=10$ autodetachment rate.

The rotational dependence of the C_2^- autodetachment rates has been measured for $v'=6$–9. The experimental results are presented in Fig. 6, where the autodetachment rates for $N'=1$–51 are plotted against $N'(N'+1)$, i.e., as a function of the rotational energy. The lifetimes of the F_1 and F_2 components were found to be the same (within experimental error) in those cases examined. Although the magnitude of the rates is primarily determined by the vibrational state of C_2^-, a strong rotational dependence—the rates almost double from $N'=1$–51—is observed. As Fig. 6 suggests the autodetachment rates within one vibrational manifold appear to depend linearly on the rotational energy of the autodetaching level. Deviations from the linear dependence are obvious only for small N' of the $v'=7$ sequence. As we will see in Sec. V D, this is explained by interference of autodetachment of the C_2^- $A\,^2\Pi_u$ state. Possible processes leading to the observed behavior of the C_2^- autodetachment rates are discussed in detail below.

C. Discussion

Autodetachment rates can be calculated using the golden rule as

$$\frac{2\pi}{\hbar}\,|\langle\psi_f|\underline{Q}|\psi_i\rangle|^2\rho\,. \tag{7}$$

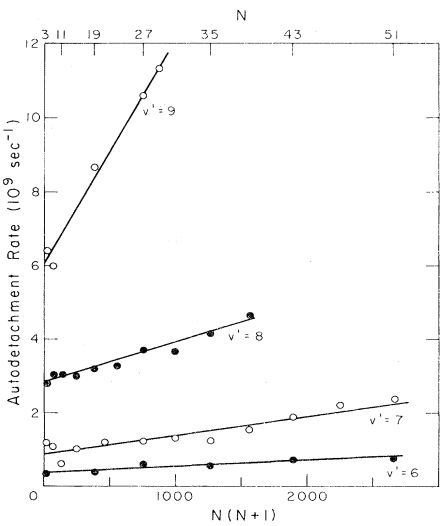

FIG. 6. Rotational dependence of the C_2^- autodetachment rates for the $B\,^2\Sigma_u^+$ vibrational levels $v'=6$–9. Typical errors are $\pm1\times10^8$ s^{-1}.

The ψ_i and ψ_f are initial- and final-state wave functions, respectively, $\underline{Q}$ is the operator corresponding to the relevant autodetachment process, and ρ is the density of final continuum states. For the photodetachment of nonpolar molecules, where the (molecule plus electron) final state basically can be treated as two free particles, the density of final states ρ is proportional to the square root of the excess energy. Autodetachment arises from terms in the Schrödinger equation usually neglected in bound-state solutions. Mechanisms that couple molecular bound states to the continuum include configuration interaction, vibration-to-electronic energy coupling, rotation-to-electronic energy coupling, or combinations of those. Whereas the first mechanism is due to correlation of the electrons (Coulomb repulsion) and thus is a pure electronic coupling, the other two arise from the coupling of nuclear and electronic motion, a breakdown of the Born-Oppenheimer approximation.

As is obvious from the potential diagram (Fig. 4), autodetachment of C_2^- due solely to configuration interaction is energetically forbidden, because the electronic energy of the C_2^- $B\,^2\Sigma_u^+$ state is smaller than the electron affinity of C_2. Thus we have to concentrate on vibration-to-electronic and rotation-to-electronic energy coupling to explain autodetachment of C_2^-. Both couplings are accomplished by terms of the nuclear kinetic-energy operator normally neglected in the Born-Oppenheimer approximation. The radial term

$$T_v=-\frac{\hbar^2}{2m}\frac{\partial}{\partial R}\bigg|_{\rm el}\frac{\partial}{\partial R}\bigg|_{\rm vib} \tag{8}$$

of the nuclear kinetic-energy operator describes vibration-to-electronic coupling, whereas the angular term

$$T_R=-\frac{\hbar^2}{2mR^2}\vec{\rm N}\bigg|_{\rm el}\cdot\vec{\rm N}\bigg|_{\rm rot} \tag{9}$$

accomplishes rotation-to-electronic coupling.[8,9] The notations $|_{\rm el}$ and $|_{\rm vib}$ indicate that the operator acts either on the electronic or rovibronic wave function.

The nuclear rotational angular momentum operator is represented here by $\vec{\rm N}$, which is equal to $\vec{\rm J}-\vec{\rm S}$. For non-Σ states, $\vec{\rm R}=\vec{\rm J}-\vec{\rm L}-\vec{\rm S}$ would be used. For autodetachment of C_2^- to be energetically allowed, the energy difference between the electron affinity of C_2 and the electronic energy of the C_2^- $B\,^2\Sigma_u^+$ state has to be provided by internal energy sources. This corresponds to either the vibrational level $v'\geq5$ if the energy came purely from vibration, or the rotational level $N'\geq79$ if the energy came purely from rotation. A loss of 79 quanta of angular momentum, as required for rotation-to-electronic coupling to be the only autodetachment mechanism, is very unlikely. Indeed no high rotational lines ($N'\geq28$) for $v'=4$ have been observed, indicating that vibration-to-electronic energy coupling is the *dominant* mechanism in C_2^- autodetachment. Under this assumption and with further approximations[8] the matrix element of Eq. (7) can be written as follows:

$$\langle \psi_f \mid T_v \mid \psi_i \rangle = -\frac{\hbar^2}{2m}\left\langle \psi_f^{\rm el}\left|\frac{\partial}{\partial R}\psi_i^{\rm el}\right.\right\rangle \times\left\langle \psi_f^{\rm vib}\left|\frac{\partial}{\partial R}\psi_i^{\rm vib}\right.\right\rangle \delta_{J_f J_i} . \quad (10)$$

Calculation of the vibronic matrix element needed for the autodetachment rate is straightforward, using wave functions generated from the C_2^- Rydberg-Klein-Rees (RKR) potentials.[5,19] Autodetachment of $C_2^- v' \geq 6$ to the $C_2\, a\, ^3\Pi + e$ continuum, as pointed out in Sec. V B, is considered to be the dominant process. In this manner we find that the ratio of the "vibronic" transition probabilities for autodetachment of $C_2^-\ B\, ^2\Sigma_u^+$, v' levels to the energetically allowed vibrational levels of the $C_2\ a\, ^3\Pi_u$ state is 1, 4.6, 12, 24, and 38 for $v'=6$, 7, 8, 9, and 10, respectively. These calculated results are in good agreement with the experimentally observed ratios of the autodetachment rates (see Table II). While vibration-to-electronic energy coupling describes the vibrational dependence of the C_2^- autodetachment rates very well, it does not easily explain the observed rotational dependence. Throughout the range of $C_2^-\ B\, ^2\Sigma_u^+$ vibrational levels probed, the rotationless negative-ion vibrational levels lie near (usually just below) the rotationless levels of the $C_2\ a\, ^3\Pi_u$ state.[5,19] Since these neutral levels may not be energetically accessible, they are not included in the vibronic transition probabilities listed above. However, a small amount of rotational energy conversion would make the additional vibrational levels allowed. The vibronic transition probabilities for these states are typically ten times greater than those quoted above, so the effect of the additional rotational energy could be amplified significantly by this process. The rotation-electronic coupling matrix elements $\langle \psi_f \mid T_R \mid \psi_i \rangle$ cannot be factored into a simple product, as was possible for $T_{\rm vib}$ in Eq. (10). Thus the calculation will be more complicated. Qualitative inspection of T_R, however, shows that it describes a coupling similar to Λ-type doubling, giving rise to coupling matrix elements proportional to $[N'(N'+1)]^{1/2}$; i.e., autodetachment rates are expected to increase in proportion to the rotational energy, which matches very well the behavior shown in Fig. 6.

Summarizing, autodetachment of the $C_2^-\ B\, ^2\Sigma_u^+$ state can be understood in terms of vibration-to-electronic and rotation-to-electronic energy coupling, where (almost) all the energy required for electron ejection is taken out of the vibrational motion, but where a few rotational quanta transferred into the electronic motion have a noticeable impact on the overall autodetachment rate.

D. Autodetachment of the $C_2^-\ A\, ^2\Pi_u$ state

The lowest excited state of C_2^-, an $A\, ^2\Pi_u$ state, which has been recently observed,[19] also can autodetach. Autodetachment of vibrational levels $v'=16$ and higher is energetically possible. Optical excitation of these levels of the $A\, ^2\Pi_u$ state has not been directly observed[19] due to poor Franck-Condon overlap with levels of the $X\, ^2\Sigma_g^+$ ground state. Perturbations in the $B\, ^2\Sigma_u^+$ state arising from the $A\, ^2\Pi_u$ state, however, mix both states and make states with substantial $A\, ^2\Pi_u$ character observable.

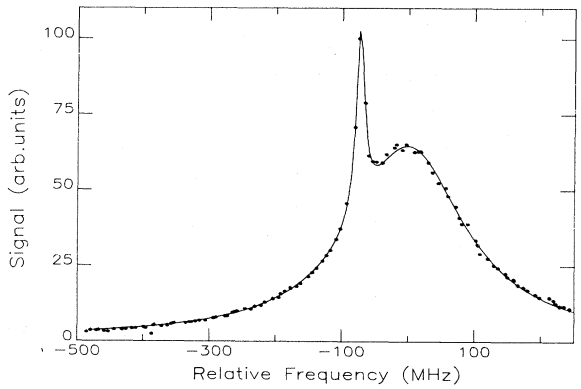

FIG. 7. Autodetachment resonances observed in C_2^-. Broad resonance (FWHM is 208 MHz) is due to autodetachment of the $B\, ^2\Sigma_u^+$ $v'=7$, $J'=23.5$, $N'=23$ level, while the narrow resonance (FWHM is 16 MHz) arises from autodetachment of the $A\, ^2\Pi_{u(3/2)}$ $v'=19$, $J'=9.5$, $N'=9$ level. Autodetachment of the $A\, ^2\Pi_u$ state can be seen due to mixing with the $B\, ^2\Sigma_u^+$ state. Point spacing is 8 MHz. Zero relative frequency corresponds to 16 336.31 $\rm cm^{-1}$.

The characteristics of the $A\, ^2\Pi_u$ state have been determined from a detailed analysis[19] of over 600 spectral lines primarily associated with the $B\, ^2\Sigma_u^+$-$X\, ^2\Sigma_g^+$ transition. Analysis of the line positions shows that while most of the lines have negligible $^2\Pi$ character, some have significant admixtures of $^2\Pi$ and some are predominantly $^2\Pi$. The analysis, which is based upon analytic techniques[32] as applied[33] in the isoelectronic N_2^+, involves iterative line assignment and least-squares fitting to a rotational Hamiltonian. The diagonal elements of the Hamiltonian are the zero-order (uncoupled) energies of the states, while the off-diagonal elements represent couplings between the $B\, ^2\Sigma_u^+$ and $A\, ^2\Pi_u$ states. Diagonalization of the Hamiltonian yields results equivalent to infinite-order perturbation theory. The squares of the eigenvector elements of the Hamiltonian matrix correspond to the fractions of $^2\Sigma$ and $^2\Pi$ character in the observed upper state. For example, Fig. 7 shows two autodetachment resonances of the $v'=7$, $v''=9$ band. The broad resonance is due to autodetachment of the $B\, ^2\Sigma_g^+$ $v'=7$, $J'=23.5$, $N'=23$ level, almost pure Σ level (99.5% Σ character), which detaches at a rate of $1.3\times10^9\ \rm s^{-1}$.

Embedded in this feature is a second, much narrower peak associated with autodetachment of the $A\, ^2\Pi_{3/2}$ $v'=19$, $N'=9$ level. This feature is only seen because the Π state is perturbed, and must be described as a mixture of 94.5% of the Π state and 5.5% of the $C_2^-\ B\, ^2\Sigma_u^+$ $v'=7$, $J'=9.5$, $N'=9$. The admixture of Σ-state character enhances the excitation probability compared to a pure $^2\Pi_u$-$^2\Sigma_g^+$ transition. The width of the Π-state resonance is primarily due to the limited resolution of the apparatus and gives an upper bound for the Π-state autodetachment rate of $1\times10^8\ \rm s^{-1}$.

The $C_2^-\ ^2\Pi$ state is described[31] by a one-electron configuration $\Pi_u \times \pi_g$ that can detach to the $C_2\ a\, ^2\Pi_u$ state upon removal of the π_g electron. Autodetachment of the $C_2^-\ A\, ^2\Pi_u$ state is a one-electron allowed process, and

thus one expects larger rates than for $B\,^2\Sigma_u^+$ autodetachment. On the other hand, assuming vibration-to-electronic coupling also for the Π state to be the dominant mechanism, vibrational matrix elements of the type occurring in Eq. (10) are much smaller for the C_2^- A state than for the B state.

If the states are not pure Σ or Π states, the autodetachment rates are an average of Σ- and Π-state rates, according to the percentage of Σ and Π character present in the observed state. Because the Π-state autodetachment rate is more than a factor of 10 slower than the Π-state rate, we expect strongly perturbed Σ states, which have a large admixture of the Π state, to have a slower autodetachment rate than unperturbed states. In the 7—9 band of C_2^-, perturbations occur around $N'=11$, where, as we can see in Fig. 6, the autodetachment rates seem to be systematically smaller than expected from the linear interpolation drawn. The autodetachment rate of the $v'=7$, $N'=11$ state (6.5×10^8 s^{-1}) is roughly 40% smaller than expected for a pure Σ $v'=7$ level. The spectroscopic analysis of the $v'=7$ band[19] indicates that this particular Σ level has only 61% Σ character. Correction for the Π character yields a pure Σ autodetachment rate of $\sim1.05\times10^9$ s^{-1}, a ratio that fits nicely into the linear overall trend.

VI. CONCLUSIONS

Resolution in crossed-beam photodetachment experiments has been limited so far to 1 part in 10^5. Taking advantage of the coaxial laser—ion-beam arrangement, we designed a new photodetachment spectrometer that improved the resolution by three orders of magnitude, but has almost the same sensitivity than the "old" crossed-beam apparatus.[5] With this coaxial beam spectrometer the C_2^- autodetachment resonances have been studied at a resolution of 10 MHz, in order to understand what coupling mechanisms lead to the autodetachment in C_2^-. Autodetachment rates have been measured for the C_2^- $v'=6-10$ vibrational levels. The measured rates are in the order of 10^7 to 10^{10} and increase roughly by a factor of 3 from one vibrational level to the next. The rotational dependence of autodetachment rates can be observed. From the observed vibrational and rotational behavior of the autodetachment rates we conclude that vibration-to-electronic energy coupling and rotation-to-electronic energy coupling are the mechanism leading to autodetachment, where most of the necessary energy to reach the continuum is taken out of the vibrational degree of freedom. Autodetachment resonances due to detachment of levels of the C_2^- $A\,^2\Pi_u$ state could be observed according to perturbations with the $B\,^2\Sigma_u^+$ state. For the Π-state autodetachment rates an upper bound, due to the resolution of the experiment, of $\gamma\leq1\times10^8$ s^{-1} can be given.

ACKNOWLEDGMENTS

One of us (U.H.) thanks the Deutsche Forschungsgemeinschaft for support during his stay at the Joint Institute for Laboratory Astrophysics (JILA). W.C.L. expresses his appreciation to the Guggenheim Foundation and to the Council on Research and Creative Work of the University of Colorado for a faculty fellowship. We are greatly indebted to Bill Hollander of the JILA Instrument shops for his assistance with the instrumental design and for his exacting fabrication work. We also wish to thank Dr. David Spence for help in designing our beam deceleration system, and Professor John Moseley for his general consultations on coaxial beam methods. This work has been supported by the National Science Foundation under Grant Nos. PHY-82-00805 and CHE-78-18424 through the University of Colorado.

*Present address: Fachbereich Physik der Universität Kaiserslautern, Postfach 3049, D-6750 Kaiserslautern, West Germany.

†Present address: School of Physics, Georgia Institute of Technology, Atlanta, Georgia 30332.

[1]G. J. Schulz, Rev. Mod. Phys. 45, 378 (1973); 45, 423 (1973); N. F. Lane, *ibid.* 52, 981 (1980).

[2]J. A. R. Samson, Phys. Rep. 28, 304 (1976).

[3]T. A. Patterson, H. Hotop, A. Kasdan, D. W. Norcross, and W. C. Lineberger, Phys. Rev. Lett. 32, 189 (1974).

[4]J. Slater, F. H. Read, S. E. Novick, and W. C. Lineberger, Phys. Rev. A 17, 201 (1978); P. Frey, F. Breyer, and H. Hotop, Phys. Lett. B 11, L589 (1978); S. E. Novick, P. L. Jones, T. J. Mulloney, and W. C. Lineberger, J. Chem. Phys. 70, 2210 (1979); P. C. Cosby, J. T. Moseley, J. R. Peterson, and J. H. Ling, *ibid.* 69, 2771 (1978).

[5]P. L. Jones, R. D. Mead, B. E. Kohler, S. D. Rosner, and W. C. Lineberger, J. Chem. Phys. 73, 4419 (1980).

[6]U. Fano, Phys. Rev. 124, 1866 (1961).

[7]J. N. Bardsley, Chem. Phys. Lett. 1, 229 (1967).

[8]R. S. Berry, J. Chem. Phys. 45, 1228 (1966).

[9]C. Duzy and R. S. Berry, J. Chem. Phys. 64, 2431 (1976).

[10]G. Herzberg, Phys. Rev. Lett. 23, 1081 (1969).

[11]U. Fano, Phys. Rev. A 2, 353 (1970).

[12]D. Dill, Phys. Rev. A 6, 160 (1972); C. Jungen and O. Atabek, J. Chem. Phys. 66, 5584 (1977); C. Jungen and D. Dill, *ibid.* 73, 3338 (1980); M. Raoult and C. Jungen, *ibid.* 74, 3388 (1981).

[13]G. Herzberg and C. Jungen, J. Mol. Spectrosc. 41, 425 (1972).

[14]P. M. Dehmer and W. A. Chupka, J. Chem. Phys. 65, 2243 (1976).

[15]G. Herzberg and A. Lagerqvist, Can. J. Phys. 46, 2363 (1968).

[16]W. C. Lineberger and T. A. Patterson, Chem. Phys. Lett. 13, 40 (1972).

[17]D. E. Milligan and M. E. Jacox, J. Chem. Phys. 57, 1952 (1969); R. P. Frosch, *ibid.* 54, 2660 (1971).

[18]D. Feldmann, Z. Naturforsch. A25, 621 (1970).

[19]R. D. Mead, U. Hefter, P. A. Schulz, and W. C. Lineberger, J. Chem. Phys. (in press).

[20]S. Leutwyler, J. Meyer and L. Misev, Chem. Phys. Lett. 91, 206 (1982).

[21]B. A. Huber, T. M. Miller, P. C. Cosby, H. D. Zeman, R. L. Leon, J. T. Moseley, and J. R. Peterson, Rev. Sci. Instrum. 48, 1306 (1977).

[22]W. H. Wing, G. A. Ruff, W. E. Lamb, and J. J. Spezeski, Phys. Rev. Lett. 36, 1488 (1976); W. H. Wing, in *Laser Spectroscopy III,* edited by J. L. Hall and J. L. Carlsten (Springer, Heidelberg, 1977), p. 69.

[23]M. Dufay, M. Carré, M. L. Gaillard, G. Meunier, H. Winter, and A. Zgainski, Phys. Rev. Lett. 37, 1678 (1976).

[24]A. Carrington and P. J. Sarre, Mol. Phys. 33, 1495 (1977).

[25]J. C. Hansen, J. T. Moseley, A. L. Roche, and P. C. Cosby, J. Chem. Phys. 77, 1206 (1982).

[26]H. Hotop, T. A. Patterson, and W. C. Lineberger, Phys. Rev. A 8, 762 (1973).

[27]H. D. Zeman, Rev. Sci. Instrum. 48, 1079 (1977).

[28]The basic approach for the design of an electron detector is to use a coaxial magnetic field along the interaction region that confines the electrons radially. The electrons will drift together with the ions and the neutrals towards the end of the interaction region where the magnetic field has a 90° turn, thus separating the electrons from the ion beam. Finally the electrons are accelerated towards the front surface of a particle detector.

[29]S. A. Lee and J. L. Hall, Appl. Phys. Lett. 25, 367 (1976).

[30]S. M. Trujillo, R. H. Neynaber, and E. W. Rothe, Rev. Sci. Instrum. 37, 1655 (1966).

[31]M. Zeitz, S. D. Peyerimhoff, and R. D. Buenker, Chem. Phys. Lett. 64, 243 (1979).

[32]R. N. Zare, A. L. Schmeltikopf, W. J. Harrop, and D. L. Albritton, J. Mol. Spectrosc. 46, 37 (1973).

[33]R. A. Gottscho, R. W. Field, K. A. Dick, and W. Benesch, J. Mol. Spectrosc. 74, 435 (1979).